Three-color mixing for classifying agricultural products for safety and quality

Fujian Ding, Yud-Ren Chen, Kuanglin Chao, and Moon S. Kim

A three-color mixing application for food safety inspection is presented. It is shown that the chromaticness of the visual signal resulting from the three-color mixing achieved through our device is directly related to the three-band ratio of light intensity at three selected wavebands. An optical visual device using three-color mixing to implement the three-band ratio criterion is presented. Inspection through human vision assisted by an optical device that implements the three-band ratio criterion would offer flexibility and significant cost savings as compared to inspection with a multispectral machine vision system that implements the same criterion. Example applications of this optical three-color mixing technique are given for the inspection of chicken carcasses with various diseases and for apples with fecal contamination. With proper selection of the three narrow wavebands, discrimination by chromaticness that has a direct relation with the three-band ratio can work very well. In particular, compared with the previously presented two-color mixing application, the conditions of chicken carcasses were more easily identified using the three-color mixing application. The novel three-color mixing technique for visual inspection can be implemented on visual devices for a variety of applications, ranging from target detection to food safety inspection.

OCIS codes: 150.0150, 120.4640, 330.1720, 330.1880.

1. Introduction

Spectroscopy and multispectral imaging techniques have been applied for military target detection, natural resources assessment, and detection of diseases, defects, and contamination for food safety and quality. At the Instrumentation and Sensing Lab (ISL), we have applied these technologies to safety inspection of agricultural products.[1–7]

Second difference, asymmetric second difference, and alternatives, which implement three-band ratios, have been used effectively in a variety of applications,[8–13] including food safety inspection.[14–17] For example, second difference preprocessing has been used for spectral data input into neural network classification of wholesome and unwholesome chicken for food safety inspection.[14] Asymmetric second difference was applied for the detection of apple surface defects and contaminations.[15]

All band ratio criteria are used in digital image processing to enhance the contrast between selected features and superfluous features. These criteria are most often implemented in multispectral imaging systems, which generally use a beam splitter to create separate channels of light directed to separate CCD sensors, with the channels passing through different wavelength bandpass filters. Ratio images are obtained by software algorithms.

The three-band ratio criterion is often used in multispectral machine vision systems to enhance the separation between diseased or contaminated agricultural products. However, multispectral imaging systems are complicated and expensive. For some small meat and poultry plants, a low-cost visual device that can be used in existing environmental conditions would be preferred.

At ISL, we are developing low-cost, optically enhanced devices that assist inspectors or plant processors in small meat and poultry plants to visually conduct inspection *in situ*.[17–19] A visual inspection assistance device based on a three-band ratio criterion consists of a pair of binoculars equipped with a special three-narrow-band interference optical filter. This device satisfies several requirements of *in situ* inspection. First, the color extraction can be

The authors are with the Instrumentation and Sensing Laboratory, Henry A. Wallace Beltsville Agricultural Research Center, ARS, USDA, Building 303, BAC-East, 10300 Baltimore Avenue, Beltsville, Maryland 20705. Y.-R. Chen's e-mail address is cheny@ba.ars.usda.gov.

Received 24 August 2005; revised 4 January 2006; accepted 7 January 2006; posted 31 January 2006 (Doc. ID 64409).

0003-6935/06/153516-11$15.00/0

easily obtained. Second, by using the binoculars, there is enough angular resolution and brightness for inspection of objects from a distance. Third, the interference filter can be implemented in the optical binocular system easily due to the small field of view (FOV) of the binocular. Fourth, it is a portable personal device, offering greater flexibility of use with a lower overall cost, compared to a multispectral imaging system. By viewing through the optical assistance device, small-plant operators can detect defective, diseased, and contaminated agricultural products, by identifying different colors resulting from the three-band ratio criterion.

In our application, we aim to develop a wearable device that can implement the three-band ratio criterion without relying on controlled narrow-band illuminating sources. Although optimizing illuminating sources is often ideal in certain applications,[20] controlled lighting is often not practical in a slaughter plant environment, and thus it is preferable to use existing illuminating sources. With special three-narrow-band optical filter device, three-band ratio interpretation can be conducted either by visual judgment, using the viewer's experience as a result of training to match target conditions to their corresponding three-band ratio colors, or by the aid of an automated interpretation program.

In this paper, a visual device to assist inspectors in identifying target conditions by utilizing a three-band ratio criterion is presented. The primary purpose of this paper is to present processes and the device needed to effectively implement the three-band ratio criterion using an optical inspection method to aid human vision. We will establish the relationship between color attributes of the colors perceived through the special binocular and the three-band ratio at three wavebands used in food safety inspection. The results can be used to train inspectors to identify the color associated with each target condition by simulating the colors of objects with known three-band ratio values. This technique for visually reading the three-band ratio is useful not only for food safety inspection, but also for target detection and for quality inspection in other fields.

2. Theory and Relation between Color Mixing and Band Ratios

A. Color Mixing

When an optical system is used in color perception, the tristimulus values X, Y, Z of an object color in the CIE 1931 color space are given by[21]

$$X = k \sum_{\lambda} \tau_{\lambda} \rho_{\lambda} H_{\lambda} \bar{x}_{\lambda} \Delta\lambda,$$

$$Y = k \sum_{\lambda} \tau_{\lambda} \rho_{\lambda} H_{\lambda} \bar{y}_{\lambda} \Delta\lambda,$$

$$Z = k \sum_{\lambda} \tau_{\lambda} \rho_{\lambda} H_{\lambda} \bar{z}_{\lambda} \Delta\lambda, \quad (1)$$

where $\bar{x}_{\lambda}$, $\bar{y}_{\lambda}$, $\bar{z}_{\lambda}$ are 1931 CIE color-matching functions, k is a normalizing factor, $H_{\lambda}\Delta\lambda$ is the spectral distribution of the flux irradiating the object, ρ_{λ} is the spectral reflectance of the object, and τ_{λ} is the transmittance of the optical system.

If three colors with tristimulus values (X_i, Y_i, Z_i) $(i = 1, 2, 3)$ and chromaticity coordinates (x_i, y_i, z_i) $(i = 1, 2, 3)$ are mixed together, a new color is produced that has chromaticity coordinates (x_m, y_m) that can be expressed as follows:

$$x_m = (k_{12}x_1 + x_2 + k_{32}x_3)/(k_{12} + k_{32} + 1),$$

$$y_m = (k_{12}y_1 + y_2 + k_{32}y_3)/(k_{12} + k_{32} + 1), \quad (2)$$

where

$$k_{i2} = (X_i + Y_i + Z_i)/(X_2 + Y_2 + Z_2) \quad (i = 1, 3). \quad (3)$$

Equation (2) shows that the chromaticity (x_m, y_m) of the mixed colors will depend only on the chromaticity coordinates (x_i, y_i, z_i) $(i = 1, 2, 3)$ of the three colors, if the quantities, k_{12} and k_{32}, remain constant. The luminance after mixing, Y_m is equal to the sum of Y_1, Y_2, and Y_3.

B. Band Ratios in Food Safety Inspection

The three-band ratio, C_{3br}, can be expressed with the indices as follows:

$$C_{3br} = E_{\lambda_1} : E_{\lambda_2} : E_{\lambda_3}, \quad (4)$$

where E_{λ_i} $(i = 1, 2, 3)$ are the energy in the unit time received by the optical sensor at λ_i $(i = 1, 2, 3)$, respectively. They can be computed as follows:

$$E_{\lambda_i} = \int_{\lambda_i - \Delta\lambda_i/2}^{\lambda_i + \Delta\lambda_i/2} F'(x_s, y_s, z_s)\tau_{\lambda}'\rho_{\lambda}H_{\lambda}'S_{\lambda}\mathrm{d}\lambda$$

$$(i = 1, 2, 3), \quad (5)$$

where F' is the geometrical function for a given optical system, where (x_s, y_s, z_s) are the coordinates of the objects in a three-dimensional (3D) Cartesian coordinate system with the optical axis of the optical system as the Z axis and the front vertex of the objective lenses as the original point, τ_{λ}' is the spectral transmission of the optical system, H_{λ}' is the spectral radiant flux distribution of the lighting source, S_{λ} is the spectral responsivity of the optical sensor, and λ_1, λ_2, and λ_3 are the central wavelengths of the three bands. Since F' is the geometrical function, which remains constant for the three different wavelength bands of the same point on the object, so C_{3br} can be expressed as

$$C_{3\mathrm{br}} = \int_{\lambda_1-\Delta\lambda_1/2}^{\lambda_1+\Delta\lambda_1/2} \tau_\lambda' \rho_\lambda H_\lambda' S_\lambda \mathrm{d}\lambda \;:\; \int_{\lambda_2-\Delta\lambda_2/2}^{\lambda_2+\Delta\lambda_2/2} \tau' \rho_\lambda H_\lambda' S_\lambda \mathrm{d}\lambda \;:\; \int_{\lambda_3-\Delta\lambda_3/2}^{\lambda_3+\Delta\lambda_3/2} \tau_\lambda' \rho_\lambda H_\lambda' S_\lambda \mathrm{d}\lambda. \tag{6a}$$

Also, as in most applications, the $\Delta\lambda_1$, $\Delta\lambda_2$, and $\Delta\lambda_3$ are so small that the band ratio can be expressed by

$$C_{3\mathrm{br}} = \tau_{\lambda_1}' \rho_{\lambda_1} H_{\lambda_1}' S_{\lambda_1} \Delta\lambda_1 \;:\; \tau_{\lambda_2}' \rho_{\lambda_2} H_{\lambda_2}' S_{\lambda_2} \Delta\lambda_2 \;:\; \tau_{\lambda_3}' \rho_{\lambda_3} H_{\lambda_3}' S_{\lambda_3} \Delta\lambda_3, \tag{6b}$$

$$C_{3\mathrm{br}} = C_{12} \;:\; 1 \;:\; C_{32}, \tag{6c}$$

where

$$C_{12} = \frac{\tau_{\lambda_1}' \rho_{\lambda_1} H_{\lambda_1}' S_{\lambda_1} \Delta\lambda_1}{\tau_{\lambda_2}' \rho_{\lambda_2} H_{\lambda_2}' S_{\lambda_2} \Delta\lambda_2},$$

$$C_{32} = \frac{\tau_{\lambda_3}' \rho_{\lambda_3} H_{\lambda_3}' S_{\lambda_3} \Delta\lambda_3}{\tau_{\lambda_2}' \rho_{\lambda_2} H_{\lambda_2}' S_{\lambda_2} \Delta\lambda_2}.$$

Based on symmetric second difference (SSD),[14] where $\lambda_3 - \lambda_2 = \lambda_2 - \lambda_1$, the normalized symmetric second difference (NSSD) can be expressed by $\Delta_2 R(C_{12}, C_{32}) = C_{12} + C_{32} - 2$. Based on asymmetric second difference (ASD),[15] we defined the normalized asymmetric second difference (NASD) by $\Delta_2 R(C_{12}, C_{32}) = k_1 C_{12} + k_2 C_{32} - 2$, where

$$k_1 = 2\,\frac{\lambda_2 - \lambda_1}{\lambda_3 - \lambda_1},\; k_2 = 2\,\frac{\lambda_3 - \lambda_2}{\lambda_3 - \lambda_1}.$$

For the normalized symmetric second difference (NSSD), k_1 and k_2 are equal to 1.0.

Equations 6(a), 6(b), and 6(c) show that the three-band ratio is independent of the geometrical functions, and, for a given system, it is only the function of the relative reflectance of the object, if the illuminating condition remains constant. This is also true for the normalized symmetric second difference and asymmetrical second difference. It can be concluded that the three-band ratio, $C_{3\mathrm{br}}$, and the normalized second difference are not sensitive to the intensity variation in the illuminating lighting or background lighting, are not sensitive to the objective distance between the optical system and the objects, and are not sensitive to the angle between the optical axis and the normal line of the object surface. Hence, our goal was to develop the relationship between the three-band ratio and the color attributes.

C. Relation between Band Ratio Criterion and Color Attributes

In this subsection, we will give the exact relationship between the three-band ratio criterion and the chromaticness of the object color perceived through an optical device.

When mixing three colors of small and equal bandwidths, $\Delta\lambda_1$, $\Delta\lambda_2$, and $\Delta\lambda_3$, Eqs. (3) and (6b) can be used to give k_{i2} as follows:

$$k_{i2} = \frac{\tau_{\lambda_1}\tau_{\lambda_2}' H_{\lambda_1} H_{\lambda_2}' S_{\lambda_2} (\bar{x}_{\lambda_i} + \bar{y}_{\lambda_i} + \bar{z}_{\lambda_i})}{\tau_{\lambda_2}\tau_{\lambda_1}' H_{\lambda_2} H_{\lambda_1}' S_{\lambda_1} (\bar{x}_{\lambda_2} + \bar{y}_{\lambda_2} + \bar{z}_{\lambda_2})}\, C_{i2} \quad (i = 1,\ 3), \tag{7a}$$

or

$$k_{i2} = c_i C_{i2} \quad (i = 1,\ 3). \tag{7b}$$

Here parameters c_1 and c_3 remain constant for the device.

In the CIELUV color space,[21] the saturation, s_{uv}^*, and hue angle, h_{uv}, of a single target are respectively defined as

$$s_{uv}^* = 13[(u' - u_n')^2 + (v' - v_n')^2]^{1/2}, \tag{8}$$

$$h_{uv} = \arctan(v^*/u^*). \tag{9}$$

In our application, s_{uv}^* and h_{uv} can be expressed as follows:

$$s_{uv}^* = \left[\left(\frac{a_1 + a_2 C_{12} + a_3 C_{32}}{a_4 + a_5 C_{12} + a_6 C_{32}}\right)^2 + \left(\frac{a_7 + a_8 C_{12} + a_9 C_{32}}{a_4 + a_5 C_{12} + a_6 C_{32}}\right)^2\right]^{1/2}, \tag{10}$$

$$h_{uv} = \arctan[(a_1 + a_2 C_{12} + a_3 C_{32})/(a_7 + a_8 C_{12} + a_9 C_{32})], \tag{11}$$

$$C_{32} = \frac{d_1 + d_2 \cos(h_{uv}) s_{uv}^* + d_3 \sin(h_{uv}) s_{uv}^*}{d_4 + d_5 \cos(h_{uv}) s_{uv}^* + d_6 \sin(h_{uv}) s_{uv}^*}, \tag{12}$$

$$C_{12} = \frac{d_7 \cos(h_{uv}) + d_8 \sin(h_{uv}) + s_{uv}^* [d_9 \cos(2h_{uv}) + d_{10} \sin(2h_{uv}) + d_{11}]}{d_{12} \cos(h_{uv}) + d_{13} \sin(h_{uv}) + s_{uv}^* [d_{14} \cos(2h_{uv}) + d_{15} \sin(2h_{uv}) + d_{16}]}, \tag{13}$$

where $a_1, a_2, \ldots, a_9, d_1, d_2, \ldots, d_{16}$ all are parameters (see Appendix A), which are functions of the

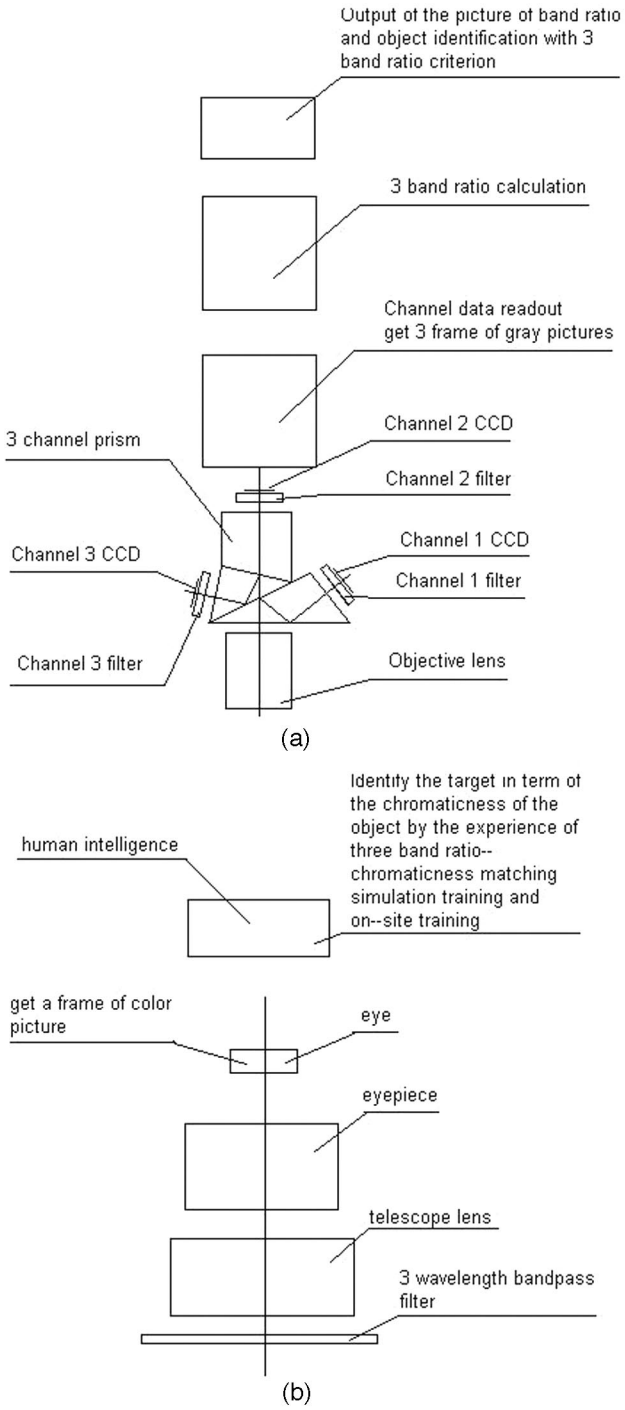

Fig. 1. Schematic of implementation of three-band ratio criterion (a) with multispectral imaging system; (b) with three-color mixing visual device.

chromaticity (x_i, y_i, z_i) $(i = 1, 2, 3)$, (x_n, y_n, z_n), and c_1 and c_3. Here, (x_n, y_n, z_n) is the chromaticity of the reference white point. The three-band ratio indices, C_{12} and C_{32}, are then only functions of the color attributes s_{uv}* and h_{uv}. So the three-band ratio and the normalized second difference are the function of s_{uv}* and h_{uv}. With Eqs. (10) and (11), the saturation and the hue of a perceived object color can be calculated in terms of its three-band ratio indices. Equations (12) and (13) can be used to calculate the three-band ratio corresponding to specified color attributes of saturation and hue. Then the three-band ratio and the normalized second difference can be performed in terms of the color attributes of the object colors.

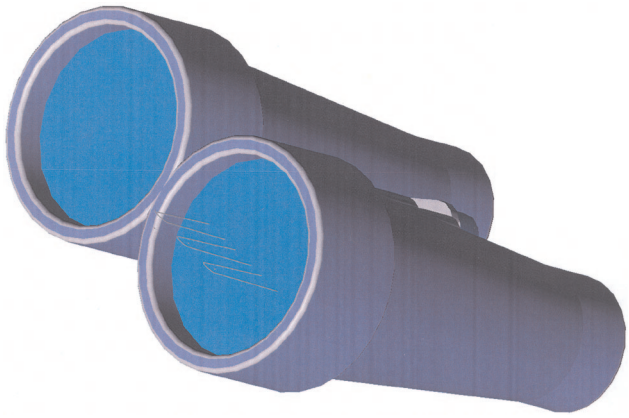

Fig. 2. (Color online) Schematic of binocular-based three-color mixing visual device.

D. Color and Chromaticness Differences Indices

Using the CIELUV color space,[21] the color difference between two targets or between a target and its background is given as

$$\Delta E(L^*u^*v^*) = [(\Delta L^*)^2 + (\Delta u^*)^2 + (\Delta v^*)^2]^{1/2}, \quad (14)$$

and the chromaticness difference index, $\Delta S'$, is defined as

$$\Delta S' = 13[(\Delta u')^2 + (\Delta v')^2]^{0.5}. \quad (15)$$

The definitions of L^*, u^*, v^*, u', and v' are given in Ref. 21. Both these indices take into account the difference in hue and saturation between two targets or a target, and the background and can be also be used as a criterion for separating target and background.

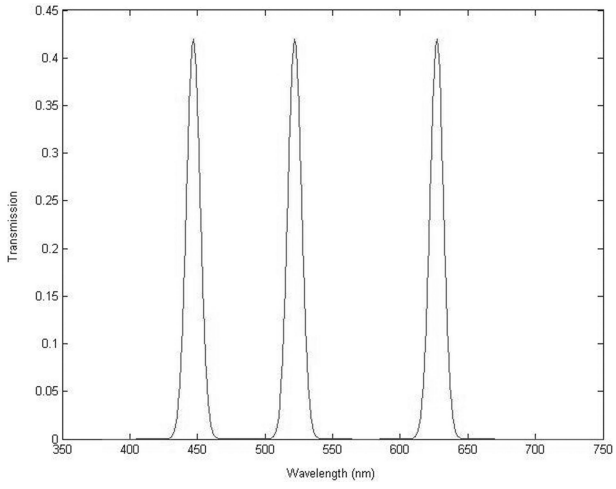

Fig. 3. Spectral transmission of the three-band filter.

3. Application to Food and Agriculture Product Inspection

A. Viewing Device and Active Lighting Used

Figures 1(a) and 1(b) show the schematics of optical devices using the three-band ratio for assisting in inspection. A pair of low-cost 8 × 32 binoculars with a 7.5 FOV can be customized with an interference three-bandpass filter in front of the objective lens, as shown in Fig. 1(b). The minimum focus distance of this binocular is 7 feet. When the operator is 2.2 m from objects being inspected, the angle of a 2 mm object for the eye is 25 mm. Figure 2 shows the schematic of this binocular. The spectral transmission of the three-bandpass filter is shown in Fig. 3.

The objects were illuminated with 5000 lx using a D65 source, the adapting is 20% of the luminance of white in the adapting field, and only light passing through the binoculars' special filters reached the viewer. The reference "white" as seen through this device is different from "white" under the D65 standard, so we finish the color-simulation with the condition that white is D65 with an adapting field luminance of 18 cd/m^2, using the revision of CIE color appearance model CIECAM97s.[22,23] This model can be used to convert from tristimulus values to perceptual attributes, while its inverse model can be used to convert from perceptual attributes back to tristimulus values.

All the results presented below are based on the conditions that (1) the optical transmissions of the visual device and the multispectral system are very similar in the visible range, and (2) the spectral energy distributions of the illuminating sources in the multispectral system application and the visual device application are CIE D65.

B. Separating Different Unwholesome Conditions of Chicken Carcasses

U.S. legislation requires USDA Food Safety and Inspection Service (FSIS) inspectors at poultry slaughter plants to inspect each poultry carcass to be sold for human consumption. There are many diseases associated with chicken carcasses that an experienced inspector must be able to determine for real-time on-line inspection.

Septicemia/toxemia (septox), a systemic disease condition, is the most common cause of carcass condemnation (removal of a bird from the processing line). Septicemia is caused by pathogenic microorganisms or their toxins in the bloodstream, while toxemia refers to a condition in which the blood contains toxins either produced by cells at a localized infection or derived from the growth of microorganisms. Septox carcasses are often dark red to bluish in color, dehydrated, stunted, or edematous.[24] Other conditions that most commonly cause carcass removal from the processing line are airsacculitis (a lung disease) and tumor (cartilaginous nodules). Inspectors also condemn carcasses for other defects that are not associated with any specific diseases, such as cadaver (resulting from improper slaughter), bruises, inflammatory process (IP), and fecal contamination. These unwholesome carcass conditions demonstrate a variety of obvious changes in skin color.

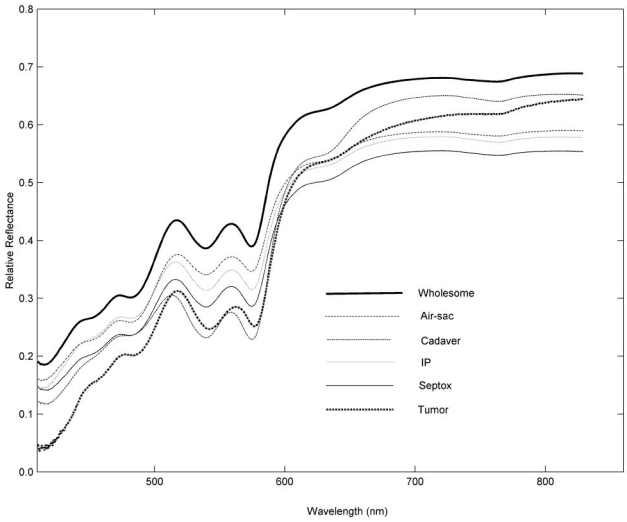

Fig. 4. Relative reflectance of chicken skin.

1. *Materials and Spectral Measurements*

A total of 467 chicken carcasses (213 wholesome, 51 airsacculitis, 80 cadaver, 51 IP, 64 septox, and 8 tumor) were obtained from a processing line at a poultry slaughter plant in Cordova, Maryland. These wholesome and unwholesome conditions were identified in the plant by USDA FSIS inspectors. Chicken carcasses were marked according to condition and placed in plastic bags to minimize dehydration during transport. Then the bags were placed in coolers, covered with ice, and transported to the ISL facility in Beltsville, Maryland, within 2 hours of removal from the processing line.

For each sample, the right breast was removed with the skin intact, and from this a 49 mm diameter circular area was cut out. The skin, approximately 4 mm thick, was removed and set aside, while the meat was sliced to a thickness of 15 mm. Before sample reflectance measurements were taken, dark background and white reference (black and white polytetrafluoroethylene, respectively) measurements were collected. To take a sample reflectance measurement, the sample (chicken meat with skin overlaid) was placed in the sample holder, and the fiber-optic probe was positioned 2 cm above the surface of the sample. Visible/near-infrared (Vis/NIR) reflectance spectra were first collected using a photodiode array spectrophotometer (Oriel Company, Stratford, Connecticut) in the wavelength range of 411.0–923.0 nm, in increments of 0.5 nm, resulting in 1024 data points per spectrum. In an effort to improve the signal-to-noise ratio, each spectrum was the average of 244 scans of the diode array, where each scan was a result of a 0.0328 s photodiode array exposure. Figure 4 shows the relative reflectance spectra of various chicken carcasses conditions.

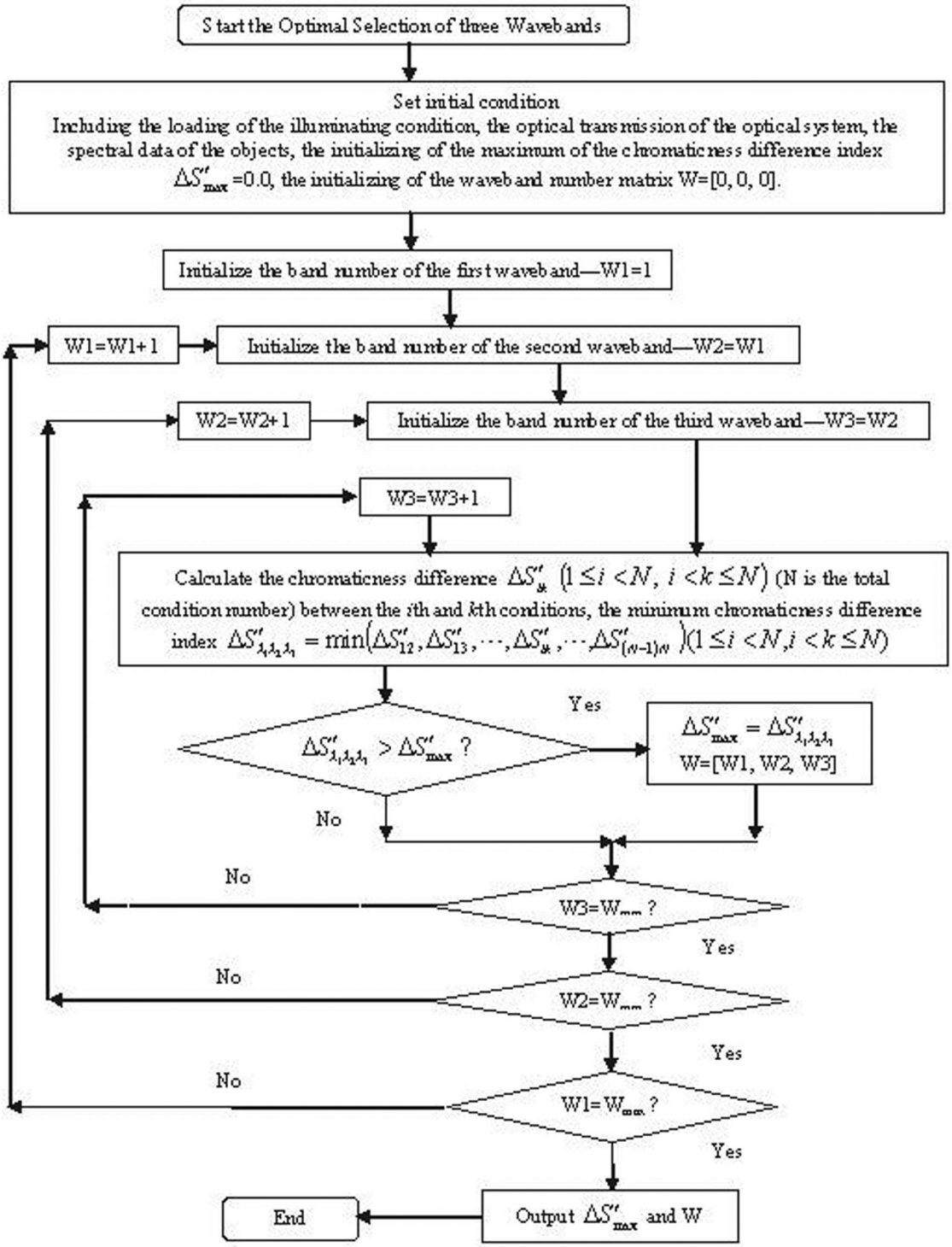

Fig. 5. Flow chart of the algorithm for the selection of the optimal three wavebands.

In this application, the average spectral data for tumor condition is corrected using the ratio between the tumor area and the total sensed area according to the following formulation:

$$\mathrm{Rt}_\lambda = \frac{A_{\mathrm{total}}}{A_{\mathrm{tumor}}} \times \mathrm{Ro}_\lambda - \left(\frac{A_{\mathrm{total}}}{A_{\mathrm{tumor}}} - 1\right) \times \mathrm{Rn}_\lambda, \qquad (16)$$

where A_{total} is the total sensed area, A_{tumor} is the area of the tumor, Rn_λ is the average reflectance for wholesome skin, Ro_λ is the average reflectance for the total sensed area including the tumor and the surrounding wholesome skin, and Rt_λ is the estimated average reflectance for the tumor area.

2. *Optimal Wavebands Selection and Color Difference for Chicken Inspection*

Searching for optimal filter wavelengths for the visual device to be used in identifying carcass conditions,

Table 1. Visual Device Optimal Wavelength of Three Bands

Target Condition		Wavelengths (nm) Band 1	Band 2	Band 3
Single-Target	Wholesome	417	462	594
	Air-sac	447	534	630
	Cadaver	414	531	648
	IP	456	588	645
	Septox	411	519	651
	Tumor	426	513	643
Multitarget		447	522	627

based on the spectral characteristics of the carcasses, is a very important first step. The criterion for separating a single carcass condition, such as wholesome, from all other conditions is to maximize the chromaticness difference index $\Delta S'$ between the wholesome carcasses and the unwholesome carcasses. For differentiating between multiple carcass conditions, the objective of waveband optimization is to select the three-waveband set $(\lambda_1, \lambda_2, \lambda_3)$ that maximizes the smallest chromaticness differences between all the multiple target conditions. The procedure of the selection of the optimal three-waveband set is similar to the selection of the optimal two-waveband set.[17–19] The flow chart of the three-waveband optimal selection is shown in Fig. 5.

Table 1 shows the optimal three-waveband sets for the single condition detection and multiple condition detection. Table 2 shows the color differences for the multitarget wavelength set (447 nm, 522 nm, and 627 nm), while Table 3 shows the parameters that were used in Equations (10), (11), (12), and (13) to obtain the values for saturation, hue, and the band ratio indices. The related parameters k_1 and k_2, used in the normalized asymmetric second difference, were 0.833 and 1.167, respectively.

Table 4 shows, for each carcass condition, the band ratio indices and the saturation and hue values for the multitarget detection wavelength set (447 nm, 522 nm, and 627 nm), along with the normalized asymmetric second difference for each condition. The cadaver condition clearly shows the smallest hue value, differing very obviously from the hue in the other conditions. The saturation of the tumor condition is greatest and has obvious differences from all the other five conditions. These factors render the cadaver and the tumor colors the most distinct from the others. According to the value of the saturation and hue in CIELUV color space, the air-sac and wholesome conditions are similar. These results are consistent with the normalized asymmetric second differences, cadaver and tumor are each very distinct from all the other conditions, and air-sac and wholesome carcasses are close to each other in terms of the normalized asymmetric second difference (last column in Table 4).

If the color difference between two different conditions is greater than a numerical value of 5.0,[25] it is considered to be easily differentiable by eye, while a value of 1.0 is considered to be only a noticeable color difference, under the CIE reference viewing condition.[25] Table 2 shows that all the six conditions can be identified. The color difference between any two different conditions is always near or greater than 5.0.

Here, the color differences resulting from the bandwidths simplification expressed in Eq. (6b) were calculated for the chicken carcasses inspection. Results

Table 2. Multitarget Color Differences Comparison

	Wholesome	Air-sac	Cadaver	IP	Septox	Tumor
Wholesome	0.0	5.05	27.4	10.2	9.39	20.2
Air-sac		0.0	29.5	12.6	9.91	15.2
Cadaver			0.0	17.2	19.7	41.1
IP				0.0	4.40	26.2
Septox					0.0	22.2
Tumor						0.0

Table 3. Parameters at Wavelength Set 447 nm, 522 nm, and 627 nm

Parameters	Values	Parameters	Values	Parameters	Values
a_1	3.6108	c_1	16.4187	d_8	−1.4087
a_2	−0.73166	c_3	2.7148	d_9	−0.34209
a_3	1.1046	d_1	2.9637	d_{10}	−0.93523
a_4	−3.2352	d_2	1.5169	d_{11}	0.09302
a_5	−0.16523	d_3	0.54976	d_{12}	0.60063
a_6	1.3714	d_4	0.82092	d_{13}	−0.13564
a_7	12.82	d_5	−0.53302	d_{14}	−0.16463
a_8	2.8639	d_6	0.36754	d_{15}	0.1785
a_9	5.1472	d_7	6.2377	d_{16}	−0.22536

Table 4. Saturation, Hue Angle, and Band Ratio at Wavelength Set 447, 522, and 627 nm

	Parameters				
Target Condition	C_{12}	C_{32}	s_{uv}*	h_{uv} (°)	$\Delta_2 R$
Air-sac	0.3810	1.911	1.256	59.14	0.548
Cadaver	0.4097	2.518	1.549	51.14	1.280
IP	0.4009	1.964	1.222	57.46	0.626
Wholesome	0.3871	1.929	1.246	58.60	0.574
Septox	0.3854	2.043	1.332	56.93	0.705
Tumor	0.2883	2.300	1.862	57.17	0.924

showed that the color differences resulted from the 10 nm bandwidths simplification are less than 1.0. Those color differences resulting from the 10 nm bandwidths simplification are very small compared with the color differences between different average chicken carcasses conditions, so small that they cannot be discriminated by human vision; consequently, bandwidth of less than 10 nm can be used in the bandwidth simplification in Eq. (6b).

Compared with using the two-color mixing application,[17,18] the identification of the air-sac condition from the wholesome condition using the three-color mixing application becomes easier because the three-band color difference is as high as 5.05, while the two-band color difference is only 3.57. For the identification of the septox condition from the IP condition, the color difference greatly improves from 2.97 to 4.40 when using the three-band application instead of the two-band application, clearly making identification of septox from IP much easier.

C. Application for Detection of Fecal Contamination on Apples

1. *Materials and Spectral Measurements*

Gala apples were collected from postharvest storage bins prior to any caliber/quality sorting or any processing treatments, such as antifungal or waxing applications, at a fruit grower in Pennsylvania (Rice Fruit Company, Pennsylvania).

Optimal wavebands were determined by analyzing data collected by a hyperspectral imaging system at ISL. For each pixel, 119 spectral bands were collected. The spectral wavelength range was 425–858 nm with about 3.6 nm intervals. Two 150 W halogen lamps provided the illumination for image collection. A white Spectralon panel with nearly 99% reflection ratio was used as a reference.

Figure 6 shows an image of four Gala apples, marked with ten regions of interest (ROIs) that were used in our application. From the hyperspectral imaging data, 69 wavebands covering the 425–675 nm region were used to reconstruct the colors as viewed under the D65 illuminating source. The ten ROIs were selected to include areas of good-smooth apple skins (a, b, e, and g); areas that were treated 1:20 dilution of fecal matter by water (c, d, f, and i); areas treated with a 1:2 dilution of fecal matter by water (h); and an area showing soil contamination (j). Figure 7 shows the average relative spectral reflectance for each of the ROIs. First, we aimed to identify the six contaminated ROIs from the four ROIs showing good-smooth apple skin.

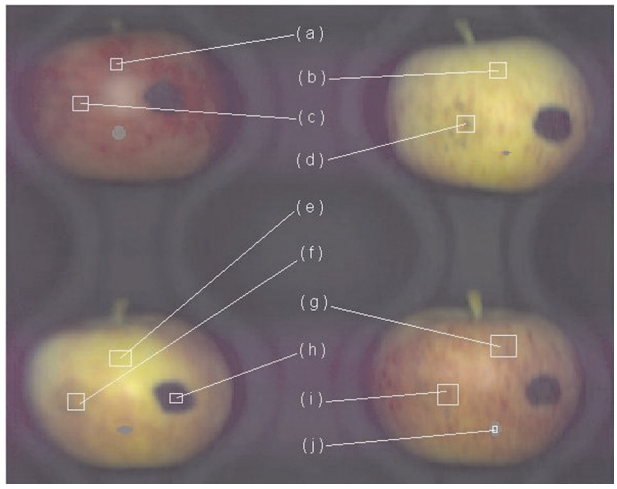

Fig. 6. Simulated color picture of one group of Gala apples in the wavelength range from 425 nm through 675 nm.

2. *Selection of Optimal Wavelengths for Apple Inspection*

For separating normal apple skin (no contamination) sites from contaminated sites, the objective of the waveband set optimization was to select the three-waveband set (λ_1, λ_2, λ_3) with the maximum of the smallest chromaticness differences between each of the normal apple ROIs and each of the contaminated apple ROIs. Three wavelengths (428 nm, 524 nm,

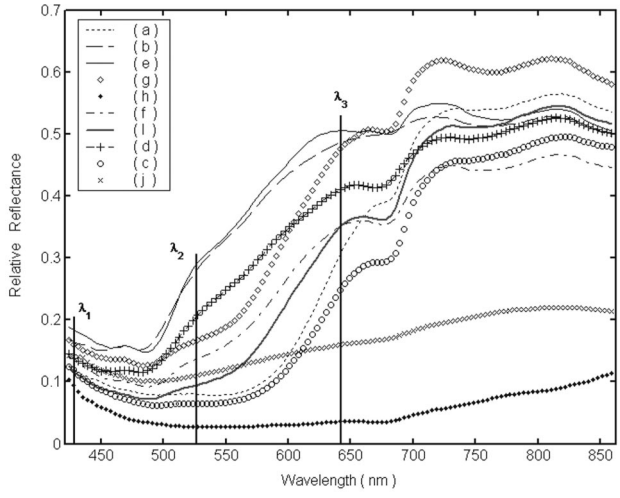

Fig. 7. Relative reflectance of contaminations on Gala apples: (a) good skin at top-left apple; (b) good skin at top-right apple; (c) 1:20 diluted fecal contamination on top-left apple; (d) 1:20 diluted fecal contamination on top-right apple; (e) good skin at bottom-left apple; (f) 1:20 diluted fecal contamination on bottom-left apple; (g) good skin at bottom-right apple; (h) 1:2 diluted fecal contamination on bottom-left apple; (i) 1:20 diluted fecal contamination on bottom-right apple; (j) soil contamination on bottom-right apple.

Table 5. Color Differences between Gala Normal Skin and Contaminated Skins at Wavelength Set 428 nm, 524 nm, and 641 nm

		ROI of the Fecal and Soil Contaminated Skins					
		(h)	(f)	(i)	(d)	(c)	(j)
ROI of Good Gala Apple Skins	(a)	59.3	21.2	8.86	42.7	10.2	45.1
	(b)	80.4	34.7	51.7	13.2	59.8	48.4
	(e)	78.6	32.3	49.3	11.4	57.5	46.7
	(g)	72.8	14.1	14.6	27.6	30.1	49.4

and 641 nm) were obtained after the waveband optimization for the multiple conditions.

A second three-wavelength set (461 nm, 630 nm, and 649 nm) was selected, which met the minimum requirement of chromaticness differences between normal apple skin ROIs and contaminated ROIs, yet the variations of the chromaticness difference among the normal apple skin sites were minimized.

3. Results for Apple Inspection for Fecal Contamination

Table 5 shows the color differences between each of the good Gala apple skins and each of the contamination sites with the mixing of the three wavebands at 428 nm, 524 nm, 641 nm. All six contamination sites can be easily identified because the color difference between any pairing of contamination and good apple skin ROIs is greater than 8.86.

For this wavelength set of 428 nm, 524 nm, and 641 nm, the training color charts corresponding to the contaminations against a background for each of the good apple skins are shown in Fig. 8. From top to bottom, the four large color rectangles are the colors of the (a), (b), (e), and (g) normal skin ROIs, respectively. Within each of the large rectangles, the three smaller rectangles from left to right show the colors of soil, 1:20 diluted fecal, and 1:2 diluted fecal contam-

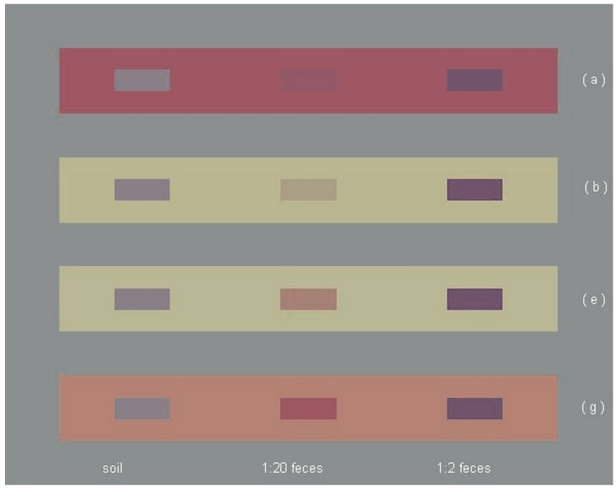

Fig. 8. Training color charts of Gala apples: (a) good skin at top-left apple; (b) good skin at top-right apple; (e) good skin at bottom-left apple; (g) good skin at bottom-right apple.

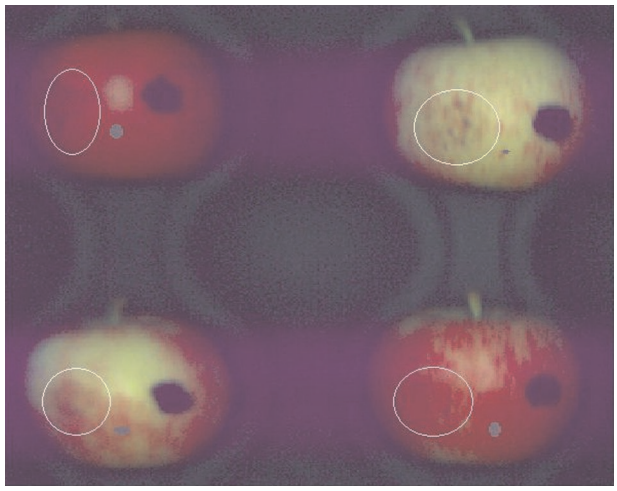

Fig. 9. Simulated picture of the group of Gala apples at wavelength set 428 nm, 524 nm, and 641 nm.

inations. Figure 8 again shows the color differences between the good apple skins and the contaminations on the apples are distinct enough for identifying the contaminations. The 1:2 fecal contamination appears dark bluish, while the soil contamination appears grayish. The 1:20 fecal contaminations have a distinct chromaticness difference from the background apple skins. Figure 9 shows the simulated image of the four apples as viewed through the optical visual device for color mixing using the three-waveband set of 428 nm, 524 nm, and 641 nm.

Table 6 shows the color differences between each of the good Gala apple skins and each of the contamination conditions at the wavelength set 461 nm, 630 nm, and 659 nm. Here, the chromaticness difference between the different good Gala apple skins is minimized, as differences between good skins and the contaminated ROIs are bigger than the minimum value. All six contamination conditions can be easily identified because the color difference between any pairing of contamination and good apple skin ROIs is greater than 5.21.

Figure 10 shows the simulated color image of the apples as viewed through the color-mixing optical visual device using the three-waveband set of 461 nm, 630 nm, and 659 nm. The 1:2 diluted fecal contaminations are easily identified and the 1:20 diluted fecal contamination can also be detected. The soil contam-

Table 6. Color Differences between Gala Normal Skin and Contaminated Skins at Wavelength Set 461 nm, 630 nm, and 659 nm

		ROI of the Fecal and Soil Contaminated Skins					
		(h)	(f)	(i)	(d)	(c)	(j)
ROI of Good Gala Apple Skins	(a)	131.7	16.9	30.7	29.5	12.9	84.9
	(b)	162.1	14.6	10.7	5.21	43.9	114.5
	(e)	169.9	21.8	12.5	9.62	51.5	122.4
	(g)	168.1	19.6	9.60	7.12	49.5	120.8

Fig. 10. Simulated picture of the group of Gala apples at wavelength set 461 nm, 630 nm, and 659 nm.

ination can also be easily detected, appearing more grayish than the fecal contaminations.

Comparing the perceived pictures through our device, Fig. 9 and Fig. 10 with the simulated color photo of Fig. 6, the three-color mixing application enhanced the chromaticness difference between different color good Gala apple skins and soil and fecal contaminations on them, despite variations in apple skin color.

4. Conclusions

In food safety and quality inspection, it is important to have systems or devices that can help to effectively separate wholesome products from diseased or defective ones. The spectroscopic three-band ratio and its alternatives are powerful tools for discriminating among two or more classes. This paper presents a visual method of implementing the three-band ratio criterion. Using a three-band-filter optical device, we showed that the extracted color is related to the three-band ratio at three narrow wavebands. With this method, the inspector can identify the target in accordance to three-band ratio criterion.

In this paper, the relationship between saturation and hue angle and three-band ratio is presented. The saturation and hue corresponding to different three-band ratio conditions of chicken carcasses are given. It was further demonstrated that the differences in the resultant mixed color among wholesome and diseased and defective chicken carcasses are large enough to be used for discrimination. We also showed that the three-waveband mixing application is more effective than two-waveband mixing in the identification of the conditions of chicken carcasses. The example of detection of soil and fecal contamination on Gala apples showed that this visual method can identify even the less obvious contamination of fecal matter with 1:20 dilution by water. In the three-color application, it was shown that the chromaticness between normal Gala apple skins and contaminations is enhanced. In some cases the chromaticess difference between different good Gala apple skins can be greatly reduced to make the identification of contamination from the wholesome skins more obvious. It was shown that it is technically feasible to develop a binocular-based inspection device to aid the accurate detection of defective, diseased, and contaminated chicken carcasses directly by human eyes. A low-cost inspection aid such as this would be useful to operators at small slaughter and processing plants. The three-color mixing technique can greatly improve the separation power of visual inspection. This technique can also be used for detection of other types of target detection if an optimized three-band ratio criterion can be implemented in visible wavelength range.

Appendix A. Derived Relationship between a_{1-9}, b_{1-3}, d_{1-16}, and (x_1, y_1, z_1), (x_2, y_2, z_2), (x_3, y_3, z_3), and (x_n, y_n, z_n)

$$a_1 = 9y_2 - w_0(x_2 + 15y_2 + 3z_2),$$

$$a_2 = 9y_1 - w_0(x_1 + 15y_1 + 3z_1),$$

$$a_3 = 9y_3 - w_0(x_3 + 15y_3 + 3z_3),$$

$$a_4 = 4x_2 - w_1(x_2 + 15y_2 + 3z_2),$$

$$a_5 = 4x_1 - w_1(x_1 + 15y_1 + 3z_1),$$

$$a_6 = 4x_3 - w_1(x_3 + 15y_3 + 3z_3),$$

$$a_7 = x_2 + 15y_2 + 3z_2,$$

$$a_8 = x_1 + 15y_1 + 3z_1,$$

$$a_9 = x_3 + 15y_3 + 3z_3,$$

$$w_0 = 9y_n/(x_n + 15y_n + 3z_n),$$

$$w_1 = 4x_n/(x_n + 15y_n + 3z_n),$$

$$d_1 = a_2a_4 - a_1a_5,$$

$$d_2 = (a_1a_8 - a_2a_7)/13,$$

$$d_3 = (a_5a_7 - a_4a_8)/13,$$

$$d_4 = a_3a_5 - a_2a_6,$$

$$d_5 = (a_2a_9 - a_3a_8)/13,$$

$$d_6 = (a_6a_8 - a_5a_9)/13,$$

$$d_7 = a_2a_3a_4 - a_1a_2a_6,$$

$$d_8 = a_1a_5a_6 - a_3a_4a_5,$$

$$d_9 = (a_1a_2a_9 - a_2a_3a_7 + a_5a_6a_7 - a_4a_5a_9)/26,$$

$$d_{10} = (a_3a_5a_7 + a_2a_6a_7 - a_1a_5a_9 - a_2a_4a_9)/26,$$

$$d_{11} = (a_1a_2a_9 - a_2a_3a_7 + a_4a_5a_9 - a_5a_6a_7)/26,$$

$$d_{12} = (a_2)^2a_6 - a_2a_3a_5,$$

$$d_{13} = a_3(a_5)^2 - a_2a_5a_6,$$

$$d_{14} = (a_2a_3a_8 - (a_2)^2a_9 + (a_5)^2a_9 - a_5a_6a_8)/26,$$

$$d_{15} = (2a_2a_5a_9 - a_2a_6a_8 - a_3a_5a_8)/26,$$

$$d_{16} = (a_2a_3a_8 - (a_2)^2a_9 + a_5a_6a_8 - (a_5)^2a_9)/26.$$

The authors thank Xuemei Zhang, Agilent Technologies, and Michael D'Zmura, University of California, Irvine, for their kind suggestion, and Diane E. Chan for assisting in the collection of spectral data for chicken carcasses.

References

1. Y. R. Chen, K. Chao, and M. S. Kim, "Machine vision technology for agricultural applications," Comput. Electron. Agric. **36**(2), 173–191 (2002).
2. Y. R. Chen and W. R. Hruschka, "On-line trials of a chicken carcass inspection system using visible/near-infrared reflectance," presented at the 1998 ASAE Annual International Meeting, Orlando, Fla., 12–15 July 1998, paper 983047.
3. Y. R. Chen and D. R. Massie, "Visible/NIR reflectance and interactance spectroscopy for detection poultry carcasses," Trans. ASAE **36,** 863–869 (1993).
4. Y.-R. Chen, "Classifying diseased poultry carcasses by visible and near-IR reflectance spectroscopy," *Optics in Agriculture and Forestry*, J. A. Deshazer and G. E. Meyer, eds., Proc. SPIE **1836,** 44–55 (1992).
5. K. Chao, Y. R. Chen, W. R. Hruschka, and F. B. Gwozdz, "On-line inspection of poultry carcasses by dual-camera system," J. Food Engr. **51**(3), 185–192 (2002).
6. M. S. Kim, A. M. Lefcourt, and Y. R. Chen, "Multispectral laser-induced fluorescence imaging system for large biological samples," Appl. Opt. **42,** 3927–3934 (2003).
7. A. M. Lefcourt, M. S. Kim, and Y. R. Chen, "Automated detection of fecal contamination of apples by multispectral laser-induced fluorescence imaging," Appl. Opt. **42,** 3935–3943 (2003).
8. R. Pu, S. Ge, N. M. Kelly, and P. Gong, "Spectral absorption features as indicators of water status in coast live oak (Quercus agrifolia) leaves, Intl. J. Remote Sens. **24,** 1799–1810 (2003).
9. S. C. Liew, A. S. Chia, and L. K. Kwoh, "Evaluating the validity of SeaWifs chlorophyll algorithm for coastal waters," presented at the 22nd Asian Conference on Remote Sensing, Singapore, 5–9 November 2001.
10. R. N. Clark, A. J. Gallagher, and G. A. Swayze, "Material absorption band depth mapping of imaging spectrometer data using a complete band shape least-squares fit with library reference spectra," JPL Publ. **90-54,** 176–186 (1990).
11. R. F. Kokaly and R. N. Clark, "Spectroscopic determination of leaf biochemistry using band-depth analysis of absorption features and stepwise linear regression," Remote Sensing Environ. **67,** 267–287 (1999).
12. R. E. Feind and R. M. Welch, "Cloud fraction and cloud shadow property retrievals from coregistered TIMS and AVIRIS imagery: the use of cloud morphology for registration," IEEE Trans. Geosci. Remote Sens. **33,** 172–184 (1995).
13. B. C. Gao and A. F. Goetz, "Extraction of dry leaf spectral features from reflectance spectra of green vegetation," Remote Sens. Environ. **47,** 369–274 (1994).
14. Y. R. Chen, B. Park, R. W. Huffman, and M. Nguyen, "Classification of on-line poultry carcasses with backpropagation neural networks," J. Food Proc. Engr. **21**(1), 33–48 (1998).
15. P. M. Mehl, Y. R. Chen, M. S. Kim, and D. E. Chan "Development of hyperspectral imaging technique for the detection of apple surface detects and contaminations," J. Food Engr. **61,** 67–81 (2004).
16. R. Lu and Y. R. Chen, "Hyperspectral imaging for safety inspection of food and agricultural products," in *Pathogen Detection and Remediation for Safe Eating,* Y.-R. Chen, ed., Proc. SPIE **3544,** 121–133 (1998).
17. F. Ding, Y. R. Chen, and K. Chao, "Two-waveband color-mixing binoculars for the detection of wholesome and unwholesome chicken carcasses: a simulation," Appl. Opt. **44,** 5454–5462 (2005).
18. F. Ding, Y. R. Chen, K. Chao, and D. E. Chan, "Two-color mixing for classifying agricultural products for safety and quality," Appl. Opt. **45,** 668–677 (2006).
19. F. Ding, Y. R. Chen, and K. Chao, "Application of color mixing for safety and quality inspection of agricultural products," in *Optical Sensors and Sensing Systems for Natural Resources and Food Safety and Quality*, Y.-R, Chen, G. E. Meyer, and S.-I. Tu, eds., Proc. SPIE **5996,** 59960R (2005).
20. M. Vriesenga, "Colored illumination for enhancing discriminability in machine vision," J. Visual Commun. Image Represent. **6**(3), 244–255 (1995).
21. G. Wyszecki and W. S. Stiles, *Color Science: Concepts and Methods, Quantitative Data and Formulas* (Wiley, 1982).
22. C. J. Li, M. R. Luo, and R. W. G. Hunt, "A revision of CIECAM97s model," Color Res. Appl. **25,** 260–266 (2000).
23. M. D. Fairchild, "Revision of CIECAM97s for practical applications," Color Res. Appl. **26,** 418–427 (2001).
24. B. P. Dey, Y. R. Chen, C. Hsieh, and D. E. Chan, "Detection of septicemia in chicken livers by spectroscopy," Poultry Sci. **82,** 199–206 (2003).
25. International Commission on Illumination, "Recommendation on uniform color spaces, color difference equations, psychometric color terms," Suppl. 2 to CIE Publ. 15 (E.-1.3.1), 1971/(TC-1.3.) (CIE, 1978).